Journal of ELECTRONIC MATERIALS, Vol. 41, No. 12, 2012
DOI: 10.1007/s11664-012-2245-9

Improved Optoelectronic Properties of Rapid Thermally Annealed Dilute Nitride GaInNAs Photodetectors

S.L. TAN,[1,3] C.J. HUNTER,[1] S. ZHANG,[1] L.J.J. TAN,[1] Y.L. GOH,[1] J.S. NG,[1] I.P. MARKO,[2] S.J. SWEENEY,[2] A.R. ADAMS,[2] J. ALLAM,[2,4] and J.P.R. DAVID,[1,5]

1.—Department of Electronic and Electrical Engineering, University of Sheffield, Mappin Street, Sheffield S1 3JD, UK. 2.—Advanced Technology Institute, Faculty of Engineering & Physical Sciences, University of Surrey, Guildford, Surrey GU2 7XH, UK. 3.—e-mail: s.l.tan@sheffield.ac.uk. 4.—e-mail: j.allam@surrey.ac.uk. 5.—e-mail: j.p.david@sheffield.ac.uk

We investigate the optical and electrical characteristics of GaInNAs/GaAs long-wavelength photodiodes grown under varying conditions by molecular beam epitaxy and subjected to postgrowth rapid thermal annealing (RTA) at a series of temperatures. It is found that the device performance of the nonoptimally grown GaInNAs p^+–i–n^+ structures, with nominal compositions of 10% In and 3.8% N, can be improved significantly by the RTA treatment to match that of optimally grown structures. The optimally annealed devices exhibit overall improvement in optical and electrical characteristics, including increased photoluminescence brightness, reduced density of deep-level traps, reduced series resistance resulting from the GaAs/GaInNAs heterointerface, lower dark current, and significantly lower background doping density, all of which can be attributed to the reduced structural disorder in the GaInNAs alloy.

Key words: Photodetector, dilute nitride, GaInNAs, annealing, defects, dark current, quantum efficiency

INTRODUCTION

Among all III–V semiconductors that can be made lattice matched to GaAs, the dilute nitride alloy, $Ga_{1-x}In_xN_yAs_{1-y}$, is particularly interesting due to the large conduction-band (CB) bowing coefficient induced by incorporating a small amount of nitrogen into GaAs. Since its proposal by Kondow et al.[1] as a material for near-infrared lasers, widespread interest followed and expanded into other optoelectronic devices including high-efficiency multijunction solar cells[2,3] and near-infrared photodetectors.[4,5] Unfortunately, growth of high-quality GaInNAs epilayers remains a challenge due to defects and other problems associated with nitrogen incorporation, the low growth temperature, and/or ion damage from the radiofrequency (RF) plasma source.[6] Many material quality and device performance issues that plagued the early development of Ga(In)NAs, such as poor photoluminescence (PL) efficiency,[7] high dark currents,[8] and short minority carrier diffusion lengths,[9] still persist today. *In situ* or postgrowth thermal annealing is often required to improve the crystal quality of GaInNAs and is widely reported to improve its optical characteristics such as PL intensity and spectral linewidth, although most of the work has focused on thin layers with N composition less than 3% for quantum well lasers,[10–14] with the exception of a recent work on solar cells.[15]

It was reported in our previous work that GaInNAs p–i–n diodes lattice matched to GaAs with low background doping concentration, low dark currents, and a photoresponse cutoff wavelength up to 1.28 μm could be achieved without postgrowth annealing.[5] However, recently a series of wafers grown under similar conditions were found to produce weak PL and devices with high dark currents and high background doping concentration (mid 10^{16} cm^{-3}). Significant improvement in PL and

(Received May 23, 2012; accepted August 26, 2012; published online September 29, 2012)

device performance was observed following a short thermal treatment by rapid thermal annealing (RTA). Although such improvement has been reported before in RTA-annealed GaInNAs devices,[14,15] we demonstrate, for the first time, that postgrowth RTA annealing enables GaInNAs photodetector structures grown under nonoptimal conditions to attain optical and electrical characteristics that are equal to or better than those of the optimally grown, unannealed structures.

EXPERIMENTAL PROCEDURES

A $Ga_{1-x}In_xN_yAs_{1-y}$ p–i–n structure was grown on (100) n^+ GaAs substrate using a solid-source molecular beam epitaxy (MBE) system as described previously.[5] The structure contains nominal In and N compositions of 10% and 3.8%, respectively, and layer structure as shown in Table I, which is similar to that of the optimally grown $Ga_{0.90}In_{0.10}N_{0.038}As_{0.962}$ sample ("wafer C") reported in Ref. 5, except with an intrinsic-region (or i-region) thickness of 1 μm instead of 0.4 μm. The n^+ AlAs layer below the n^+ GaAs cladding was designed to be an etch-stop layer. Although the growth conditions were broadly similar to those reported in Ref. 5, the growth temperature of the GaInNAs epilayer was modified slightly to 420°C instead of 450°C in order to maintain mirror-like surface morphology. The growth parameters for the GaInNAs epilayer were the same as previously reported, with a growth rate of about 0.56 μm/h, RF power of 180 W, and N_2 flow rate of 0.2 sccm. During growth of the GaInNAs layers, the output beam of the N_2 plasma source was passed through a pair of deflection plates biased at 400 V to deflect ions away, such that only N atoms reach the wafer surface. However, the use of deflection plates over a wide range of bias voltages was found to have only a marginal effect on the crystal and optical quality of dilute nitride materials grown in our MBE system. The GaAs cladding layers were grown at 590°C at a rate of 0.5 μm/h, similar to the previous growth conditions.[5] The unintentional background doping in the i-region was found by capacitance–voltage (C–V) measurements to be at mid 10^{16} cm^{-3}, much higher than the $\sim 10^{14}$ cm^{-3} achieved previously.[5] This suggests that the growth conditions were not optimal, possibly due to problems with the N_2 plasma source or incorporation of unwanted impurities. It is not unusual for dilute nitride wafers grown under nominally similar conditions to differ in material quality, which has been found to be very sensitive to the condition of the N_2 RF plasma source, the growth chamber, and the temperature variation on the substrate holder.[16]

Thermal annealing was carried out on four wafer pieces in N_2 ambient using RTA. The samples were capped with GaAs substrates during the annealing process to prevent arsenic desorption from the GaAs top cladding, and annealed at 700°C, 750°C, 800°C, and 850°C for 30 s, which was considered the optimum duration as no further improvement in PL intensity was observed in samples annealed for longer durations up to 90 s. x-Ray diffraction (XRD) rocking curve and PL measurements were performed on the samples before device fabrication. XRD reciprocal-space mapping analysis was not performed on the samples because the lattice mismatch between the GaInNAs epilayer and GaAs is small, i.e., -6.0×10^{-4}. From previous analysis, strain relaxation is not expected to occur in such GaInNAs structures with a thickness of around 1 μm.

The samples were processed into variable-area, circular mesa diodes with optical access window on top of the mesa without antireflective coating. Current–voltage (I–V) and C–V measurements were performed on the variable-area devices using a picoammeter and an LCR meter, respectively. Photoresponse measurements were performed on packaged devices using a grating-based (1-μm-blazed, 600 grooves/mm) monochromator and standard lock-in detection technique to measure the photocurrent density, and a Hamamatsu G8376-03 GaInAs PIN photodiode with known responsivity to measure the optical power density incident upon the device, from which the responsivity and external quantum efficiency (EQE) of the device can be obtained over the relevant spectral range. Internal quantum efficiency (IQE) is determined by dividing the EQE by $(1 - R)$, where R is the reflection coefficient, which is assumed to be similar to that of GaAs at ~0.32 over the measured spectral range.

Table I. Structural details of the studied samples

Doping Type/ Material	Nominal Thickness (nm)
p^+ GaAs	500
p^+ GaInNAs	50
i-GaInNAs	1000
n^+ GaInNAs	50
n^+ GaAs	300
n^+ AlAs	100
n^+ GaAs	200

RESULTS AND ANALYSIS

An important task is to ensure that the thermal annealing did not change the In and N contents in the GaInNAs epilayer. The XRD spectra of the as-grown and highest-temperature-annealed (850°C) samples revealed negligible change in the splitting between the substrate and epitaxial peaks, which correspond to N composition of 3.9 to 4.0% given an In composition of 10%. The GaInNAs epilayer peak of the 850°C-annealed sample showed a narrower linewidth than that of the as-grown sample, suggesting that any lattice defects or compositional fluctuations in GaInNAs may be reduced by postgrowth annealing.

Secondary ion mass spectroscopy (SIMS) measurements performed on the as-grown and 850°C-annealed samples also confirmed that annealing did not cause outdiffusion of In and N, and their concentrations were similar in the as-grown and annealed samples. SIMS was also used to identify the presence of impurities that may affect the background doping concentration in the GaInNAs active layer. A number of dopant species were tested and found to be below the SIMS detection level. Unexpectedly, oxygen impurities were found in the GaInNAs epilayers in both the as-grown and 850°C-annealed samples, at a concentration of about 2×10^{17} atoms cm^{-3}. The presence of oxygen in the GaInNAs epilayers was possibly caused by oxide contamination in the MBE vacuum chamber. A gas purifier was installed in our MBE system to filter the N_2 supply for the plasma source. However, the gas purifier was later found to be not in optimum condition. Hence, the oxygen impurities most likely originated from the N_2 source. Oxygen spikes were also detected at the epilayer/substrate interface of the samples in this work as well as that of the as-grown $Ga_{0.90}In_{0.10}N_{0.038}As_{0.962}$ in Ref. 5, which can be attributed to incomplete removal of native oxide from the GaAs substrate.

Doping profiles estimated from *C–V* measurements in Fig. 1 show that the unintentional background doping of the as-grown and annealed samples remains high—between 2.9×10^{16} cm^{-3} and 4.3×10^{16} cm^{-3}—in all the samples except the 700°C-annealed sample, which has its background doping reduced to 1.7×10^{16} cm^{-3}. A significant reduction in the background doping to $\sim 1 \times 10^{15}$ cm^{-3} was achieved in the 850°C-annealed devices, enabling full depletion of close to 1 μm at −0.5 V. This background doping level is comparable to that of a recently reported n^+–i–p^+ solar cell device which achieved depletion of 1.2 μm after 30-s RTA annealing at 910°C.[15] Among the notable differences between this work and Ref. 15 are the higher nitrogen content (>3%), lower annealing temperature, and bandgap smaller than 1 eV in our devices. Although the exact cause of the significant background doping reduction is unclear, the ease with which it could be achieved, i.e., by RTA annealing for 30 s, suggests that it is possibly the result of interaction or compensation of defects present in the GaInNAs layer, rather than the physical removal of any extrinsic doping species by thermally induced outdiffusion. A possible explanation by Ptak et al.[17] suggested that thermally induced compensation between acceptor and donor defects could be responsible for the reduction of high unintentional background doping in GaInNAs material grown at temperatures below 510°C, after a 30-min slow anneal at 650°C. It is possible that a fast anneal at a higher temperature by RTA (as in this work) could also enable such defect compensation.

In Fig. 2, the forward dark current densities of the as-grown and 700°C- to 800°C-annealed devices are plotted as a function of voltage. The ideality factor of all the devices is approximately between 1.4 and 1.5, which is similar to that of the optimally grown, unannealed GaInNAs with a range of N contents which we previously reported in Ref. 5. This ideality factor indicates that the forward dark current of the GaInNAs devices is enabled by both diffusion and recombination processes. At forward bias >0.3 V, the *I–V* curve of the as-grown sample in this work and that of the as-grown $Ga_{0.90}In_{0.10}N_{0.038}As_{0.962}$ sample in Ref. 5 exhibit a large series resistance and an ideality factor >4. This anomaly was also observed in the GaAs/GaInNAs diodes reported by Jackrel et al.[3] Given that the forward

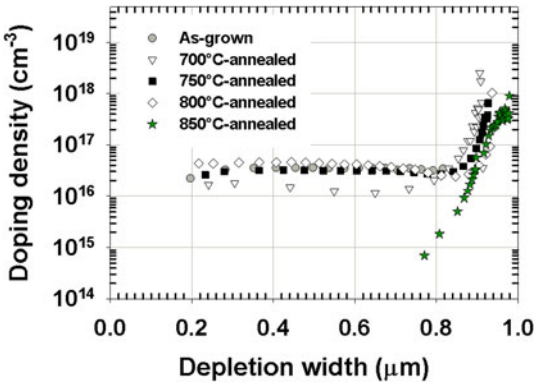

Fig. 1. Doping profiles of the as-grown and 700°C- to 850°C-annealed devices estimated from *C–V* curves. The data points for the as-grown and 700°C- to 800°C-annealed devices correspond to voltage steps of 1 V from zero bias, whereas the 850°C-annealed devices were biased in 0.1 V steps between zero and 1 V, and in 1 V steps thereafter.

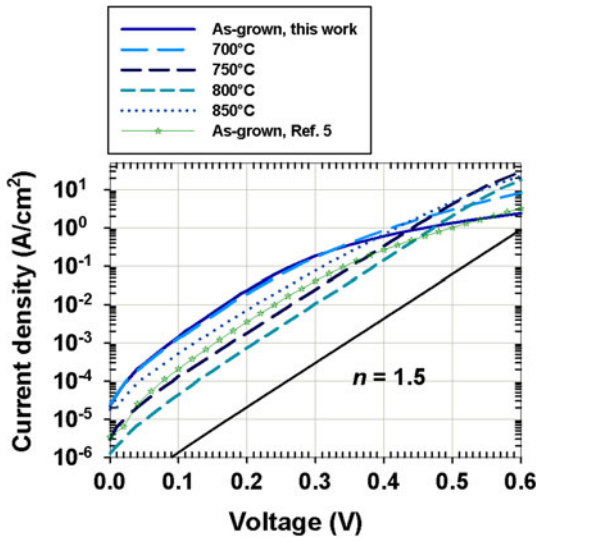

Fig. 2. Forward dark currents as a function of bias voltage of the as-grown and 700°C- to 850°C-annealed devices (lines) plotted against that of the as-grown $Ga_{0.90}In_{0.10}N_{0.038}As_{0.962}$ sample in Ref. 5 (open symbols), and a line calculated from the diode equation with an ideality factor of 1.5.

I–V and the low-resistance ohmic contacts scale with the device active area, the series resistance is believed to originate from the bulk epilayer. However, because the as-grown structure has highly doped cladding layers and a high background doping in the i-region, it is unlikely that any impurities within the GaInNAs epilayer would have a significant effect on the bulk resistance. A possible cause for current suppression in forward I–V is trapping of charge in the potential notch resulting from discontinuity in the CB or valence band (VB) in a heterojunction.[18] The GaAs/GaInNAs band alignment is known to be of type I,[19] and band discontinuities at the n-GaInNAs/n-GaAs and p-GaInNAs/p-GaAs heterointerfaces would result in a potential spike/notch in the CB and VB, respectively. However, the bandgap and hence band discontinuities are not expected to differ significantly between the as-grown and annealed samples. Furthermore, although the large series resistance is almost eliminated by the 800°C annealing, it appears to make a small comeback in the 850°C-annealed sample. A more likely explanation is that impurities or defects at the GaInNAs/GaAs heterointerface result in undesired charge-trapping effects under forward bias condition, which are improved by annealing at an optimal temperature.

By taking the natural logarithm of the forward I–V in Fig. 2, $\ln(J)$, and extrapolating the linear region to zero bias, the reverse saturation current density, J_0, for each sample can be extracted, as compared in Table II. The corresponding bandgap energy, E_g, is obtained from room-temperature (RT) PL peaks (Fig. 3). J_0 decreases exponentially with increasing bandgap energy (E_g) between the 700°C- and 800°C-annealed devices. This is an expected behavior as J_0 is a function of the square of the intrinsic carrier concentration, $n_i^2 \propto \exp(-E_g/kT)$. J_0 in a p–n junction diode is given by[20]

$$J_0 = \frac{qn_i^2 D}{NL} \propto \frac{L}{\tau}, \qquad (1)$$

where D and L are the minority carrier diffusivity and diffusion length, respectively, N is the equilibrium majority carrier concentration, and τ is the minority carrier lifetime. The increased J_0 of the 700°C-annealed device compared with that of the as-grown device is consistent with the small decrease in the background doping concentration (i.e., N in Eq. 1) as shown in Fig. 1, although it could also be due to a net increase in L/τ. Despite having the largest E_g among all the samples, the J_0 of the 850°C-annealed devices appears to be only marginally lower than that of the as-grown devices. Again, this is consistent with the significant decrease in the background doping concentration of the 850°C-annealed sample, although there could be a net increase in L/τ as well.

The RT PL spectra of the as-grown and annealed samples, excited with the 532 nm line of a diode-pumped solid-state (DPSS) laser at excitation power density of 550 W/cm^2, are shown in Fig. 3. The PL line shapes were found to be insensitive to the excitation power density between ~50 W/cm^2 and 550 W/cm^2. Changes in the PL intensity and line shape were only observed at annealing temperatures above 750°C, at which point the PL peak became narrower, stronger in intensity, and blue-shifted with increasing annealing temperature. We believe that the blue-shift of the PL peaks is caused by the change in bandgap due to structural changes in the GaInNAs alloy induced by annealing rather than due to outdiffusion of N, since no changes in the In and N contents were detected by XRD and SIMS measurements. Since postgrowth annealing has been reported to promote a change of the N-bonding configuration from Ga-N to In-N in GaInNAs, leading to a blue-shift of the PL peak,[21,22] it is possible that, during this thermally induced atomic rearrangement process, defects that contribute to the high background doping are compensated or displaced.

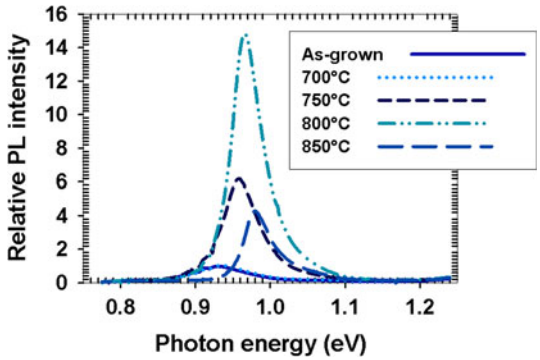

Fig. 3. RT PL peaks of the 700°C- to 850°C-annealed samples, relative to that of the as-grown sample.

Table II. Reverse saturation current densities of the GaInNAs devices extrapolated from the forward I–V plots in Fig. 2

Sample	As-Grown, Ref. 5	As-Grown, This Work	700°C	750°C	800°C	850°C
J_0 (μA/cm^2)	12.2	69.6	99.6	9.41	3.14	65.4
E_g (eV)	0.97	0.930	0.931	0.958	0.966	0.980

Also shown are the corresponding bandgap energies obtained from PL.

The PL peak intensity increases almost linearly with annealing temperature from 700°C, reaching a maximum value of ~15 relative to that of the as-grown sample, followed by a decrease of almost four times leading to the much weaker PL peak in the 850°C-annealed sample. However, the full-width at half-maximum (FWHM) of the RT PL spectra narrows rapidly with increasing annealing temperature, resulting in a 2× narrowing of the PL peak at 850°C to 43.8 meV, compared with that of the as-grown sample (89.7 meV) as well as the $Ga_{0.90}In_{0.10}N_{0.038}As_{0.962}$ sample in Ref. 5 (87.8 meV). The best RT PL FWHM to date was 28 meV, close to that of GaAs, for a slow-annealed GaInNAs layer with E_g around 0.98 eV, although the epilayer thickness is unknown.[11] To the best of our knowledge, the PL FWHM of the 850°C-annealed sample is among the best reported to date for a ~1-μm-thick bulk GaInNAs layer with E_g around 0.98 eV at RT.

At RT, the PL spectra of all the samples showed a weak transition around 0.81 eV, which is only visible in Fig. 3 on a logarithmic scale. The intensity of the ~0.81 eV peak relative to the main peak at a given laser excitation power increases rapidly with decreasing temperature. At a given temperature, the variation of the position and line shape of the ~0.81 eV emission with laser excitation intensity is negligible, suggesting that the emission is a transition from a deep level to the band edge. Figure 4 shows the PL spectra of the as-grown and 800°C-annealed samples at ~12 K, normalized to the intensity of the ~0.81 eV peak. It is obvious that the ~0.81 eV peak affects the measured FWHM of the band-edge transition peak in the as-grown sample, which is improved by postgrowth annealing. The ~0.81 eV emission has been attributed to the gallium vacancy and arsenic interstitial pair defects, As_i-V_{Ga}, in GaAs grown at low temperatures around 400°C.[23] Since the ~0.81 eV emission is also present in the electroluminescence spectra but absent in samples etched down to the n^+ GaAs substrate, it is believed that this deep radiative center originates from defects in the GaInNAs epilayer of our samples.

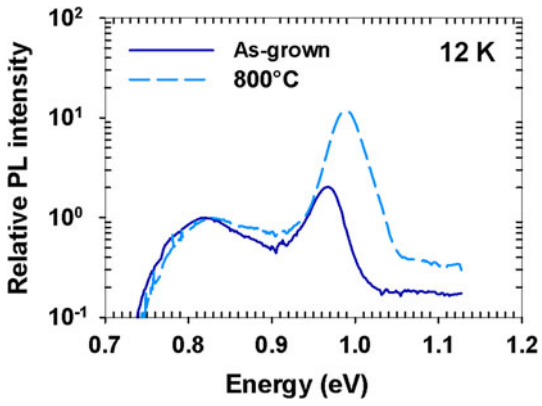

Fig. 4. PL peaks of the as-grown and 800°C-annealed samples at ~12 K, relative to the secondary peak around 0.80 eV.

Figure 5a compares the reverse dark current densities (J_R) of all the samples as a function of peak electric field, calculated by fitting the C–V results using a three-layer abrupt p^+–i–n^+ model based on the one-dimensional (1D) Poisson equation. Also shown in the figure is the dark current of the optimally grown $Ga_{0.90}In_{0.10}N_{0.038}As_{0.962}$ sample in Ref. 5. The corresponding J_R as a function of bias voltage is shown in Fig. 5b, where the smaller breakdown voltage of the Ref. 5 device is due to its thinner i-region. At electric field between 100 kV/cm and 400 kV/cm, the reverse dark current of the 750°C-annealed device is comparable to that of the Ref. 5 device, while those of the as-grown, 700°C-, and 850°C-annealed devices are about an order of magnitude higher. It is interesting to note that the 800°C-annealed device produces almost an order of magnitude lower reverse dark current compared with the Ref. 5 device, over the relevant field range. In addition, the differential resistance–area product, R_dA, at a given reverse bias increases with annealing temperature up to 800°C, above which it decreases. Between the as-grown and the 800°C-annealed devices, the zero-bias resistance–area product, R_0A, increases by 4.5×, while the peak R_dA increases by slightly over 40×.

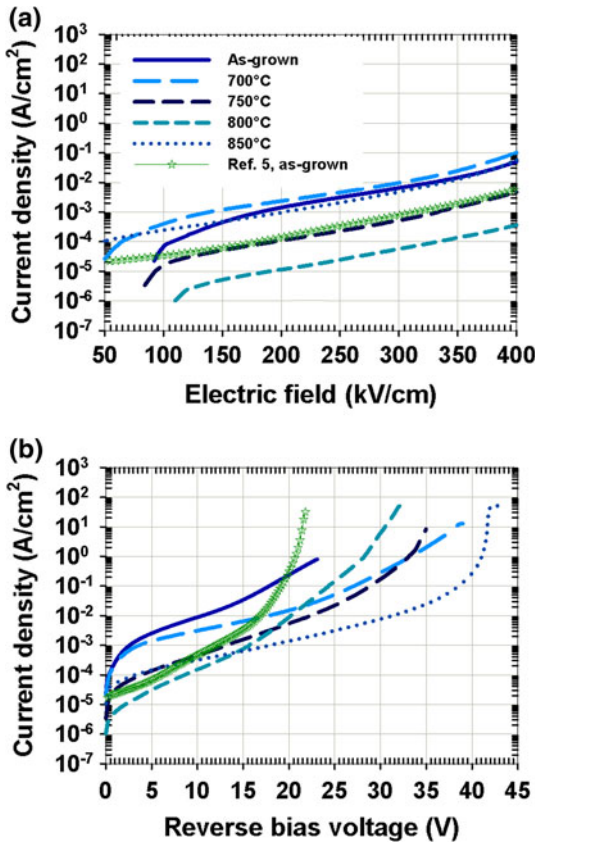

Fig. 5. Reverse dark currents as a function of (a) electric field and (b) reverse bias voltage of the as-grown and 700°C- to 850°C-annealed devices (lines) plotted against the dark current of the as-grown $Ga_{0.90}In_{0.10}N_{0.038}As_{0.962}$ sample in Ref. 5 (open symbols).

In Fig. 6, the reverse dark currents of GaInNAs devices with different depletion widths at a field of 100 kV/cm as a function of E_g are compared. It was previously reported that dark current at a given electric field decreases exponentially with increasing E_g in GaInNAs devices irrespective of the In and N compositions.[24,25] The solid circles in Fig. 6 denote the devices taken from the as-grown GaInNAs wafers reported in Ref. 5, all of which have a depletion width of about 0.4 μm at 100 kV/cm, while the triangles denote the 700°C-, 750°C-, and 800°C-annealed devices in this work, with a depletion width of ~0.2 μm at 100 kV/cm. The two sets of data appear to follow different exponential trends. The dark currents of the as-grown devices represented by the solid circles can be fitted with the expression $A\exp(-E_a/kT)$, where A is a constant, k is the Boltzmann constant, E_a is the activation energy taken to be equal to E_g, and T is the temperature, which is close to 300 K. This indicates that the band-to-band generation current is the dominant mechanism in these optimally grown devices. However, the dark currents of the nonoptimally grown devices represented by the triangular symbols cannot be fitted using a similar expression with $E_a = E_g$ and T = 300 K, suggesting that the activation energy is much smaller than the bandgap and that the dominant generation process is due to emission from deep-level traps. The high dark current in the 850°C-annealed device relative to the other devices can be attributed to the increased J_0 as well as the Shockley–Read–Hall (SRH) process. It is well known that the SRH component of the reverse current is proportional to the depletion width (W),[20] which is about 4× wider in the 850°C-annealed devices at zero bias compared with the other samples.

Figure 7 shows the C–V characteristics of the as-grown and 800°C-annealed devices modulated with a 55 mV test signal at frequencies from 10 kHz to 1 MHz. The presence of nonradiative recombination traps or deep levels is obvious in the as-grown sample, as indicated by the frequency dispersion of the C–V in Fig. 7a. With decreasing modulation frequency, the maximum capacitance in the as-grown sample moves towards more negative bias voltages. This phenomenon is an indication of positive traps being charged at small reverse bias, increasing the capacitance, and then discharged at larger reverse bias, decreasing the capacitance. The presence of such traps is consistent with the nonradiative traps due to Ga vacancies and N interstitials reported in GaInNAs samples grown under nonoptimal conditions,[15,26] which are known to degrade the PL efficiency. In the 800°C-annealed device, the C–V dispersion is negligible over the measured frequency range, indicating reduced trap levels and densities, leading to a much higher PL peak intensity as aforementioned. The frequency-induced C–V dispersion of the 850°C-annealed device (not shown in figure) is smaller than that of the as-grown sample and becomes negligible at larger reverse bias voltages above 1 V. This observation indicates that new traps have been introduced by the 850°C process, which explains the reduced PL peak intensity in the 850°C-annealed sample compared with that annealed at 800°C.

A further investigation into the radiative recombination efficiency can be made by plotting the integrated electroluminescence (IEL) intensity of the GaInNAs devices as a function of forward injection current on a log–log scale, as shown in

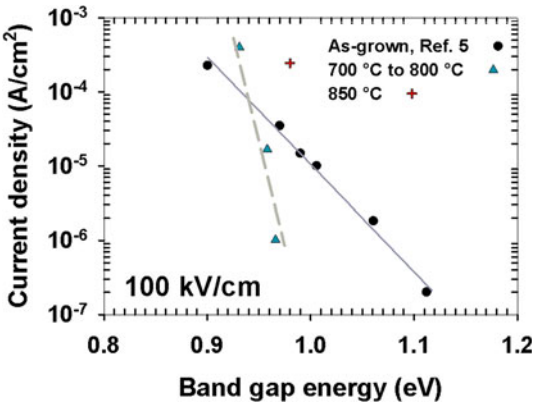

Fig. 6. Reverse dark current densities versus E_g of the annealed GaInNAs devices in this work compared with those of the optimally grown devices reported in Ref. 5, at a field of 100 kV/cm. The solid and dashed lines represent trend lines for the data points.

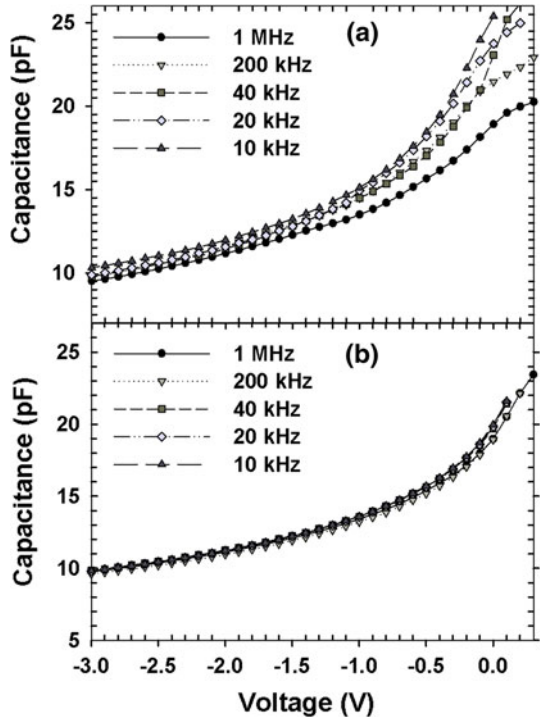

Fig. 7. C–V characteristics of 100-μm-diameter (a) as-grown and (b) 800°C-annealed GaInNAs devices as a function of modulation frequency.

Fig. 8, which is normalized to 1 at injection current of 100 mA. A slope of 1 on the log–log plot of IEL intensity versus injection current indicates very efficient radiative recombination, whereas a slope of 2 indicates that defect-related nonradiative recombination is dominant.[28] It can be seen in Fig. 8a that the IEL intensity of the as-grown devices in this work and the as-grown $Ga_{0.90}In_{0.10}N_{0.038}As_{0.962}$ devices in Ref. 5 show a superlinear dependence on the injection current. Nonradiative recombination is dominant in the as-grown and 700°C-annealed samples, while in the higher-temperature-annealed samples, radiative recombination becomes dominant with increasing annealing temperature as well as injection current. This observation suggests that deep levels, which degrade radiative recombination efficiency, exist in all the samples, but are reduced by the RTA annealing above 700°C.

The EQE spectra of the as-grown, 800°C- and 850°C-annealed devices at zero bias and −1 V were determined from the responsivity measurements described in Sect. II and are plotted in Fig. 9. The cutoff wavelength for each sample, which is estimated from the −3 dB point relative to the peak intensity of the photoresponse, blue-shifts from about 1325 nm in the as-grown sample to 1270 nm in the 850°C-annealed samples, consistent with the blue-shift of the PL peaks discussed previously in Fig. 3. It is interesting to note that the peak EQE of the 850°C-annealed device, i.e., 25% at zero bias, is more than twice that of the as-grown and 800°C-annealed devices, which have zero-bias EQEs of 11% and 8%, respectively, despite the identical GaInNAs absorber layer thickness in all the samples. This marked difference in EQEs suggests that

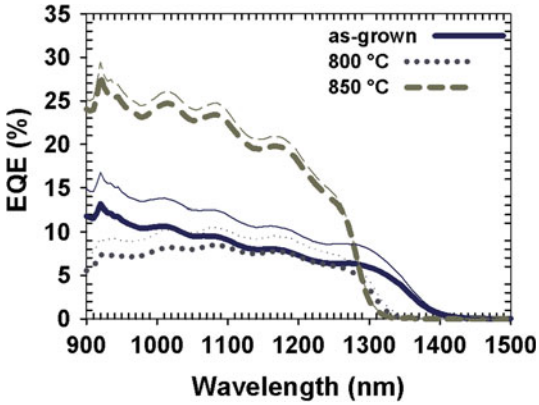

Fig. 9. EQE spectra of the as-grown, 800°C- and 850°C-annealed devices at zero bias (thick lines) and at −1 V (thin lines) where the 850°C-annealed device is fully depleted.

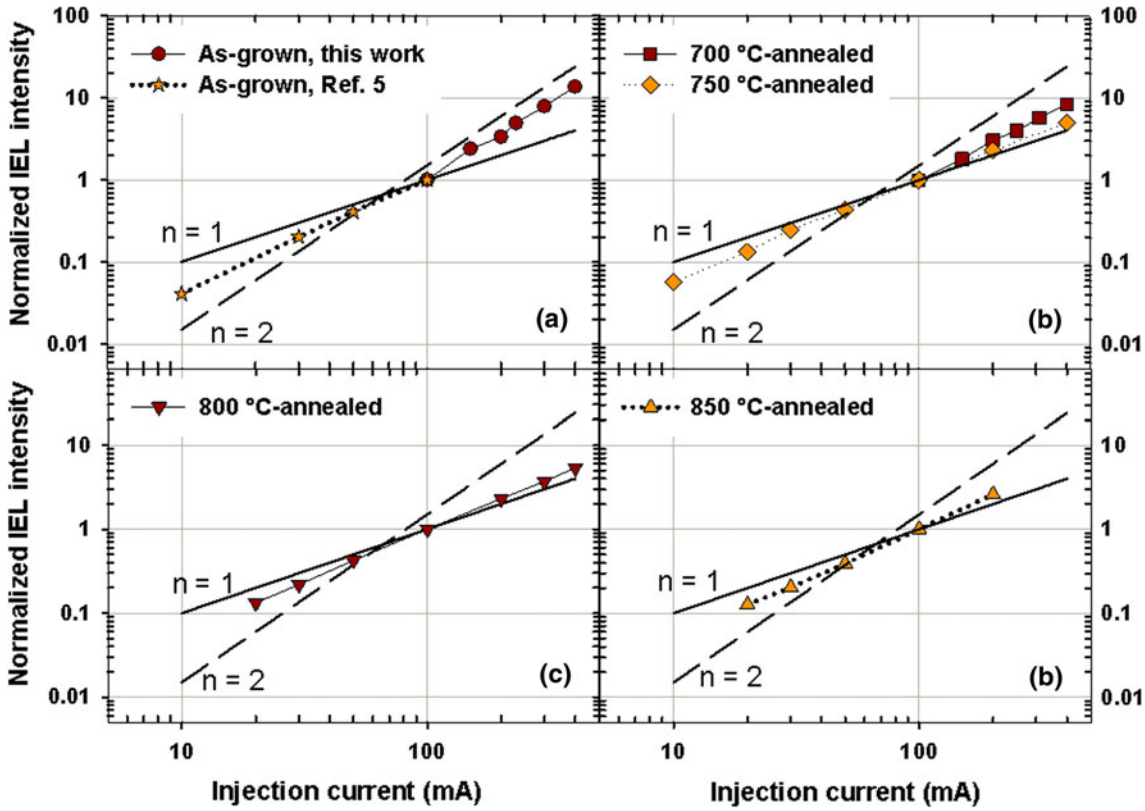

Fig. 8. RT IEL intensity as a function of injection current of the (a) as-grown sample compared with that of Ref. 5, (b) 700°C- and 750°C-, (c) 800°C-, and (d) 850°C-annealed devices, normalized to 1 at 100 mA and plotted on a log–log scale between two lines with a gradient of 1 (solid) and 2 (dashed), respectively. The IEL data for the "As-grown, Ref. 5" device in (a) is obtained from the work in Ref. 27.

the minority carrier diffusion length is shorter than the thickness of the undepleted GaInNAs epilayer (i.e., about 750 nm at 0 V) in the as-grown and 800°C-annealed devices, which have a high unintentional background doping in the *i*-region. It is well known that wider depletion widths help improve the carrier collection efficiency of diodes with short minority carrier diffusion lengths, and this is evident in the case of the 850°C-annealed device in Fig. 9.

The photocurrent of the 850°C-annealed device at an illumination wavelength of 1064 nm (absorbed in the GaInNAs p^+–i–n^+ layers) remained constant at reverse bias voltages above 0.5 V, where the *i*-region is fully depleted. The photocurrent of the 800°C-annealed device, in contrast, increased almost linearly with increasing reverse bias voltage, indicating an increase in field-assisted collection efficiency with the gradual movement of the depletion edge towards the top p^+ cladding layer. This behavior is consistent with the higher unintentional doping concentration (at mid 10^{16} cm^{-3}) in the *i*-region of the 800°C-annealed sample and suggests that the background dopant is likely to be *p*-type. Further evidence for a *p*-type background dopant is provided by the *I*–*V* characteristics of variable-sized mesa diodes from the 800°C-annealed sample, where area scaling of *I*–*V* was only observed in mesas etched below the i/n^+ junction, suggesting that a *p*–*n* junction was formed between *i*-GaInNAs and n^+-GaInNAs. Although it has been suggested that, at substrate temperatures below 500°C, the unintentional background doping in MBE-grown GaInNAs material is *n*-type,[17] the *p*-type background dopant in our as-grown sample could be due to the effect of *in situ* annealing for an hour during the growth of the top GaAs cladding layer at 590°C.

From the EQE spectra in Fig. 9, the absorption coefficients of the samples can be calculated, given the GaInNAs p^+–i–n^+ absorbing layer thickness determined by *C*–*V* and SIMS measurements. The exponential tails of the absorption coefficient spectra at photon energies below E_g were found to follow Urbach's rule given by[29]

$$\alpha(E) = \alpha_0 \exp\{[E - E_g(T)]/E_0(T)\}, \qquad (2)$$

which describes an exponential energy dependence for photon energies, E, near the absorption edge, with a characteristic width, $E_0(T)$, at a temperature T. The typical value for E_0 in GaAs and most semiconductors is about 10 meV at RT. A larger E_0 indicates disorder-induced energy band tails due to impurities in the material. By fitting to the Urbach tails of the absorption spectra using Eq. 2, the E_0 of the as-grown sample was found to be 16 meV, which was reduced to 10 meV in the 800°C- and 850°C-annealed samples, as shown in Fig. 10. It is evident from the change in E_0 that annealing reduces the effect of structural and thermal disorder in the GaInNAs material.

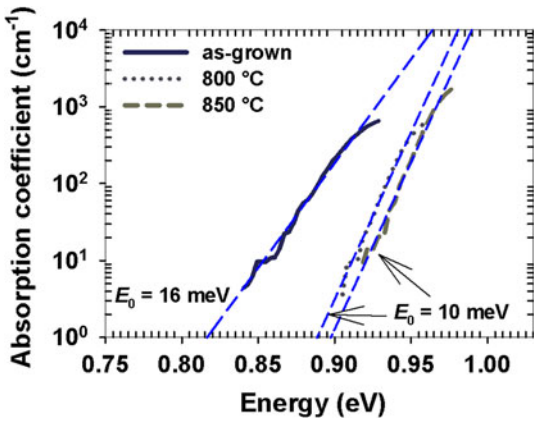

Fig. 10. Fits to the absorption coefficient spectra of the as-grown, 800°C- and 850°C-annealed devices in the Urbach-tail region.

CONCLUSIONS

We have investigated the effects of postgrowth RTA on the electrical and optical characteristics of nonoptimally grown $Ga_{0.9}In_{0.1}N_{0.038}As_{0.962}$ p^+–i–n^+ structures. Oxygen impurities were found in both the as-grown and annealed samples, although it is unclear whether oxygen plays a part in the high unintentional background doping in the as-grown sample or its subsequent compensation after thermal annealing. It is believed that, owing to the short duration, the RTA annealing process did not physically remove any extrinsic dopant from the GaInNAs epilayers nor change the In or N concentration, as confirmed by the SIMS profiles, but rather induced structural changes in the GaInNAs material which led to a blue-shift in bandgap energy with increasing annealing temperature and compensation of the acceptor-type defects at sufficiently high temperature. The decrease in the characteristic width of the Urbach tails of the annealed samples to a value typical of GaAs is an indication that annealing reduces the structural disorder in nonoptimally grown GaInNAs material. Annealing was also found to improve the radiative recombination efficiency and reduce deep-level traps with increasing temperature up to 800°C, beyond which new trap levels appeared. However, a radiative deep center at ~0.81 eV, related to defects in the GaInNAs epilayer, is present in all the samples despite annealing. Short minority carrier diffusion lengths are a persistent problem in both the as-grown and annealed samples and could only be circumvented by having a wide depletion width enabled by the significantly reduced background doping density in the 850°C-annealed devices. However, the drawback of a wide depletion width is the increase of the SRH-dominated dark current. The background doping density of $\sim 1 \times 10^{15}$ cm^{-3} is the lowest achieved so far in 1-μm-thick GaInNAs epilayers with a bandgap smaller than 1 eV. In short, this study has demonstrated the improvement in

optoelectronic properties of GaInNAs material that can be achieved by RTA, as well as the trade-offs that should be considered when postgrowth annealing is applied to GaInNAs photodetectors.

ACKNOWLEDGEMENTS

This work was funded by Engineering and Physical Sciences Research Council (EPSRC) Grants No. EP/E065007/1 and EP/E063632/1. The authors thank Dr Alison Chew and Dr David Sykes of Loughborough Surface Analysis Ltd. for SIMS measurements and useful discussion.

REFERENCES

1. M. Kondow, K. Uomi, A. Niwa, T. Kitatani, S. Watahiki, and Y. Yazawa, *Jpn. J. Appl. Phys.* 35, 1273 (1996).
2. D.J. Friedman, J.F. Geisz, S.R. Kurtz, and J.M. Olson, *J. Cryst. Growth* 195, 409 (1998).
3. D.B. Jackrel, S.R. Bank, H.B. Yuen, M.A. Wistey, J.S. Harris, A.J. Ptak, S.W. Johnston, D.J. Friedman, and S.R. Kurtz, *J. Appl. Phys.* 101, 114916 (2007).
4. E. Luna, M. Hopkinson, J.M. Ulloa, A. Guzmán, and E. Muñoz, *Appl. Phys. Lett.* 83, 3111 (2003).
5. J.S. Ng, W.M. Soong, M.J. Steer, M. Hopkinson, J.P.R. David, J. Chamings, S.J. Sweeney, and A.R. Adams, *J. Appl. Phys.* 101, 064506 (2007).
6. J.S. Harris, S.R. Bank, M.A. Wistey, and H.B. Yuen, *IEE Proc. Optoelectron.* 151, 407 (2004).
7. T.K. Ng, S.F. Yoon, S.Z. Wang, W.K. Loke, and W.J. Fan, *J. Vac. Sci. Technol. B* 20, 964 (2002).
8. W.K. Loke, S.F. Yoon, S. Wicaksono, and B.K. Ng, *Mater. Sci. Eng. B* 131, 40 (2006).
9. S.R. Kurtz, A.A. Allerman, E.D. Jones, J.M. Gee, J.J. Banas, and B.E. Hammons, *Appl. Phys. Lett.* 74, 729 (1999).
10. T. Kitatani, K. Nakahara, M. Kondow, K. Uomi, and T. Tanaka, *J. Cryst. Growth* 209, 345 (2000).
11. M. Kondow and T. Kitatani, *Jpn. J. Appl. Phys.* 40, 108 (2001).
12. S. Shirakata, M. Kondow, and T. Kitatani, *J. Phys. Chem. Solids* 64, 1533 (2003).
13. M. Kondow, T. Kitatani, and S. Shirakata, *J. Phys.: Condens. Matter* 16, S3229 (2004).
14. W.K. Cheah, W.J. Fan, S.F. Yoon, B.S. Ma, T.K. Ng, R. Liu, and A.T.S. Wee, *Semicond. Sci. Technol.* 21, 808 (2006).
15. I.R. Sellers, W.-S. Tan, K. Smith, S. Hooper, S. Day, and M. Kauer, *Appl. Phys. Lett.* 99, 151111 (2011).
16. M. Henini, *Dilute Nitride Semiconductors* (Oxford: Elsevier, 2005), pp. 5–6.
17. A.J. Ptak, D.J. Friedman, and S. Kurtz, *J. Vac. Sci. Technol. B* 25, 955 (2007).
18. C.M. Wu and E.S. Yang, *J. Appl. Phys.* 51, 2261 (1980).
19. M. Kondow, T. Kitatani, S. Nakatsuka, M.C. Larson, K. Nakahara, Y. Yazawa, M. Okai, and K. Uomi, *IEEE J. Select. Top. Quant. Electron.* 3, 719 (1997).
20. A. Zemel and M. Gallant, *J. Appl. Phys.* 64, 6552 (1988).
21. S. Kurtz, J. Webb, L. Gedvilas, D. Friedman, J. Geisz, J. Olson, R. King, D. Joslin, and N. Karam, *Appl. Phys. Lett.* 78, 748 (2001).
22. J.-M. Chauveau, A. Trampert, K.H. Ploog, and E. Tournié, *Appl. Phys. Lett.* 84, 2503 (2004).
23. P.W. Yu, G.D. Robinson, J.R. Sizelove, and C.E. Stutz, *Phys. Rev. B* 49, 4689 (1994).
24. S.L. Tan, S. Zhang, W.M. Soong, Y.L. Goh, L.J.J. Tan, J.S. Ng, J.P.R. David, I.P. Marko, A.R. Adams, S.J. Sweeney, and J. Allam, *IEEE Electron Dev. Lett.* 32, 919 (2011).
25. L.J.J. Tan, W.M. Soong, J.P.R. David, and J.S. Ng, *IEEE Trans. Electron Devices* 58, 103 (2011).
26. W. Li, M. Pessa, T. Ahlgren, and J. Decker, *Appl. Phys. Lett.* 79, 1094 (2001).
27. W. M. Soong (Ph.D. dissertation, University of Sheffield, 2009).
28. S. Sanguinetti, D. Colombo, M. Guzzi, E. Grilli, M. Gurioli, L. Seravalli, P. Frigeri, and S. Franchi, *Phys. Rev. B* 74, 205302 (2006).
29. C.W. Greeff and H.R. Glyde, *Phys. Rev. B* 51, 1778 (1995).